Fast Relaxation Modes in Model Polymeric Systems

R. C. Picu* and M. C. Pavel

Department of Mechanical, Aerospace and Nuclear Engineering, Rensselaer Polytechnic Institute, Troy, New York 12180

Received August 30, 2001; Revised Manuscript Received November 19, 2001

ABSTRACT: The fast β stress relaxation modes in a model polymeric melt are investigated by means of nonequilibrium molecular dynamics simulations. The stress is computed on the atomic level by accounting for both bonded and nonbonded interatomic interactions. The system evolution is traced during the loading and relaxation periods, and the mechanisms of stress production are identified. Stress relaxation takes place by several modes, each corresponding to specific atomic-scale structural changes. The β relaxation corresponds to the return to isotropy of the atomic distribution in the neighborhood of a representative atom and encompasses a quasielastic mode (β1) and a slower mode (β2). A diffusion-like process governs the β2 mode. The β1 mode is nonexponential and accounts for roughly 50% of the total atomic-scale stress drop during relaxation. The β2 mode is exponential and leads to a smaller stress drop, but it takes longer to complete than β1. Both β modes involve only local structural changes, and their time constants are independent of the molecular weight of the chains. These are simple thermally activated processes that do not involve cooperative relaxations and whose temperature dependence can be described by an Arrhenius equation. Furthermore, it is shown that the time constant for the exponential mode, β2, can be derived from equilibrium simulations based on the fluctuation−dissipation theorem and a continuum model of diffusion in the neighborhood of a representative atom. This shows that the nonequilibrium system is in the linear-response regime during this relaxation stage.

1. Introduction

Stress production in polymeric systems is understood at present in terms of a model in which chains are regarded as entropic springs in tension.[1−3] The configurational entropy variation associated with the stretching of a chain leads to a retractive force or a stress on the material scale. By this fundamental assumption, the stress defined on the molecular scale is purely entropic. Furthermore, it is assumed that the macroscopic deviatoric stress is produced by bonded interactions only, whereas nonbonded interactions lead to a hydrostatic stress component.

An alternative description of stress production in which stress is computed on the atomic scale was recently advanced.[4−11] This formulation is based on computer simulations of model polymeric systems and has been used both to reformulate the molecular theory and to test the validity of some of its main assumptions. For example, it was shown that the deviatoric stress is essentially due to excluded-volume interactions, that nonbonded interactions are as important in terms of deviatoric stress production as bonded interactions, and that the bonds are in compression rather than in tension as conjectured in the molecular theory. The entropic nature of the atomic-level stress results from the model rather than from being conjectured.[12]

The atomic-level stress can also be evaluated in a coordinate system tied to a generic bond belonging to the chain backbone (the "intrinsic" coordinate system). This coordinate system is therefore mobile. The two definitions of stress, computed in the global (macroscopic) and intrinsic frames, are equivalent. Specifically, the macroscopic stress can be written as the sum of "stresslets" (intrinsic stress tensors) rotated in the global coordinate system.[10] The essential property of the intrinsic stress tensors is their insensitivity to deformation when the system is above the glass transition temperature and at late times during the relaxation process. Furthermore, the stress-optical coefficient (SOC) representing the ratio of a measure of bond orientation, $P_2 = {}^1/_2\langle 3\cos^2\theta_b - 1\rangle$ (where θ_b is the angle defining bond orientation) to the global stress can be expressed in terms of intrinsic stresses.[7,13] It must be noted that the definition used here for the SOC is slightly different from the macroscopic definition according to which the SOC is the ratio of birefringence to the global stress.

The relaxation of the stress computed on the molecular scale is assumed to be associated with the return to isotropy of the orientations of the chain segments. Segments are preferentially oriented during melt deformation. Stress relaxation is usually described by a Prony series in which each exponential corresponds to a relaxation mode. Modes with various time constants are associated with the reorientation of chain segments having various lengths. Because the representation of each chain segment as an entropic spring is based on a statistical description, the segments must be long enough for the statistics to be meaningful. This imposes a lower bound on the range of segment lengths that can be considered. In turn, this limits the range of perturbation wavelengths that can be represented by this model. Mechanisms operating on a scale smaller than the smallest chain segment considered in the model are not captured. For example, the fast β relaxation modes related to local, atomic-scale structural perturbations cannot be captured by the molecular formulation.

The atomic-level stress, computed on the scale of a bond, equally represents relaxation modes associated with long- and short-range structural changes. The stress relaxation history computed in atomistic simulations is qualitatively similar to that observed in experiments for stress at the macroscopic scale. At early times (or high frequencies), the β modes are dominant. The subsequent modes (or at low frequencies) are of the α type and can be described by a Prony series. The intrinsic stress shows a small variation within the β

10.1021/ma0115949 CCC: $22.00
Published on Web 01/26/2002

regime. At later times, during the α relaxation, the intrinsic stress tensor becomes time- and deformation-independent. This leads to a constant stress-optical coefficient.

The work presented here aims to identify the mechanisms associated with the β modes and to predict their time constants. The paper is organized as follows: A description of the model and the algorithm employed are presented in the next section; an overview of the structural changes taking place in the melt is presented in section 3; and in sections 4 and 5, respectively, the $\beta 1$ and $\beta 2$ regimes are analyzed. The conclusions are summarized in section 6.

2. Model and Simulation Framework

Model. The present investigation is based on computer simulations of model systems consisting of dense collections of molecules. The molecules are represented by a "pearl necklace" type of model in which the beads represent atoms linked into chains by stiff linear springs simulating covalent bonds. Most results reported here were obtained from a monodisperse system of molecules with 11 atoms per chain (number of bonds $N_b = 10$). Simulations have also been performed with systems having 4, 61, and 201 atoms per chain ($N_b = 3$, 60, and 200, respectively) to investigate the scaling of various parameters with the chain length. The covalent bonds between the pair of atoms of each molecule are represented by the quadratic potential

$$u_b(r) = \frac{1}{2}\kappa(r - b_0)^2 \tag{1}$$

and all nonbonded atoms interact with a truncated Lennard-Jones potential. Here, r denotes the distance between any pair of atoms, and b_0 is the undeformed bond length. The spring constant κ has a value corresponding to $\kappa b_0^2/k_B T = 267$, and $b_0 = 1$. In the present simulations, the nonbonded interactions are represented by a purely repulsive Lennard-Jones potential with cutoff radius $R_c = 2^{1/6}$ (WCA potential). The units of the problem are those imposed by the Lennard-Jones potential.

Periodic boundary conditions are used in the simulations as is customary in molecular dynamics. The basic cell referred to a Cartesian system is, in the equilibrium state, a cube of dimension L. There are N atoms per unit cell, which leads to a reduced density $\rho = N/L^3$. The initial configuration of the system of chains is obtained by performing self-avoiding random walks on a dummy BCC lattice that fills the undeformed simulation cell. Only configurations with a random bond orientation are retained. Then, a high-temperature equilibration is performed by molecular dynamics to obtain a proper melt structure. A typical simulation with the system $N_b = 10$ contained 1540 atoms, whereas the long-chain system ($N_b = 200$) contained $N = 5025$ atoms.

The algorithms used to integrate the equations of motion as well as to implement the thermostat are those due to Berendsen et al.[14] The position of a particle at time $(t + \Delta t)$ is obtained from its positions at times t and $(t - \Delta t)$ by

$$\mathbf{x}(t+\Delta t) = (1 + \xi)\mathbf{x}(t) - \xi\mathbf{x}(t-\Delta t) + \xi\frac{\mathbf{f}}{m_0}\Delta t \tag{2}$$

where the force $\mathbf{f}$ acting on the atom in question is determined from the atomic positions at time t. The scaling factor ξ is given by the equation

$$\xi = \left[1 + \frac{\Delta t}{\Omega}\left(\frac{T_o}{T(t-\Delta t/2)} - 1\right)\right]^{1/2} \tag{3}$$

where T_o is the target temperature and $T(t-\Delta t/2)$ is calculated using the velocities at time $(t - \Delta t/2)$ obtained from

$$\mathbf{v}(t-\Delta t/2) = \frac{\mathbf{x}(t) - \mathbf{x}(t-\Delta t)}{\Delta t} \tag{4}$$

The parameter Ω controls the speed of response of the algorithm to a temperature perturbation. For our simulations, performed under high-strain-rate−high-energy input conditions, this parameter is taken as $\Omega = 10\Delta t$. For this value, it was verified that the temperature at the onset of relaxation is the target temperature and remains so throughout the relaxation. The time step of integration, Δt, is kept constant for the whole loading−relaxation history and is equal to 0.001. It was verified that a further decrease in Δt did not affect the results.

Simulations were performed under nonequilibrium conditions. The melt deformation is induced by a volume-preserving elongational deformation of the unit cell. During such a deformation in the stretch direction x_1, the cell size is modified according to

$$\begin{aligned} L_1 &= L(1 + \dot{\epsilon}t) \\ L_2 &= L/(1 + \dot{\epsilon}t)^{1/2} \\ L_3 &= L/(1 + \dot{\epsilon}t)^{1/2} \end{aligned} \tag{5}$$

where $\dot{\epsilon}$ is the deformation strain rate. All simulations reported here were performed with a strain rate $\dot{\epsilon} = 0.1$ and with a total deformation of the cell in the stretch direction is 20%. The periodic boundary conditions remained unchanged during deformation.

To reduce the noise in measured quantities, the calculation had to be repeated N_c number of times using independent initial conditions and the results averaged over all runs. The results reported here were obtained by averaging over $N_c = 200$ simulations for the 11-atoms-per-chain system and over $N_c = 12$ replicas for the 201-atoms-per-chain system.

Atomic-Level Stress in Global Coordinates. The stress t_{ij} in the melt expressed in the global coordinate system tied to the simulation cell is computed using the virial stress formula[15]

$$Vt_{ij} = -NkT\delta_{ij} + \frac{1}{2}\sum_{m=1}^{N}\langle\sum_{n=1}^{N_m} r_{mn}^{-1}u'_{mn}(r_{mn})r_{mni}r_{mnj}\rangle \tag{6}$$

where $V = L^3$ is the volume of the unit cell, r_{mn} is the length of the vector $\mathbf{r}_{mn}$ between interacting atoms m and n and has components r_{mni}, and $u' = du/dr$. The first sum is taken over all atoms in the system, whereas the second is over all N_m atoms interacting with atom m at time t in a given simulation. The contributions to the stress of both bonded and nonbonded interactions are considered, with u_{mn} representing the respective potential. The kinetic term $-NkT$ is assumed to contribute to the hydrostatic stress only as the thermal velocities are much higher than those due to the deformation of

the simulation cell. The angular brackets represent averaging over all N_c replicas.

The nonkinetic contribution to the global stress of a representative atom m at time t in a given simulation is therefore

$$\sigma_{ij}^{m} = \frac{1}{2V}\sum_{n=1}^{N_m} r_{mn}^{-1} u'_{mn}(r_{mn}) r_{mni} r_{mnj} \tag{7}$$

Atomic-Level Stress in Intrinsic Coordinates. The intrinsic stresses are defined for each atom in an intrinsic coordinate system $\tilde{x}_i$ with axis $\tilde{x}_1$ tied to one of the covalent bonds of that atom (inset to Figure 3).[9] The atomic-level stress due to atom m in eq 7 can be expressed in the intrinsic coordinate system by a simple rotation of the stress tensor as

$$\tilde{\sigma}_{rs}^{m} = \sigma_{ij}^{m}\, a_{ri}^{m}\, a_{sj}^{m} \tag{8}$$

where $a_{ri}^{m} = \mathbf{a}_r^m \cdot \mathbf{e_i}$ represents components of the rotation matrix relating the global and intrinsic coordinate systems for atom m. The intrinsic stress tensor $\tilde{\sigma}_{rs}$ is obtained by averaging $\tilde{\sigma}_{rs}^{m}$ over all N atoms in the system and over all N_c simulations. The intrinsic stress is a cylindrical tensor in which the only nonzero components are $\tilde{\sigma}_{11}$ and $\tilde{\sigma}_{22} = \tilde{\sigma}_{33}$.

The Stress Optical Coefficient. The SOC or the ratio of birefringence to stress is defined here as the ratio of P_2 to the atom-based stress.[16] The global stress difference defined by $\sigma = t_{11} - (t_{22} + t_{33})/2 = (^3/_2)^{\mathrm{D}}t_{11}$is expressed in terms of the deviatoric intrinsic stresses $^{\mathrm{D}}\tilde{\sigma}_{ii} = \tilde{\sigma}_{ii} - (\tilde{\sigma}_{11} + \tilde{\sigma}_{22} + \tilde{\sigma}_{33})/3$ as[7,16]

$$\sigma = \sigma^{\mathrm{b}} + \sigma^{\mathrm{nb}} = CP_2(\theta_{\mathrm{b}}) \tag{9}$$

where

$$C = \frac{3}{2}[\rho_{\mathrm{b}}\, {}^{\mathrm{D}}\tilde{\sigma}_{11}^{\mathrm{b}} + \rho_{\mathrm{a}} D\, {}^{\mathrm{D}}\tilde{\sigma}_{11}^{\mathrm{nb}}] \tag{10}$$

The global atom-based stress in eq 9 is computed as the sum of contributions due to bonded and nonbonded interactions and is proportional to P_2 in the α-relaxation regime. The proportionality constant C is the inverse of the SOC ($C = 1/\mathrm{SOC}$). The bond and atom number densities are represented by ρ_{b} and ρ_{a}, respectively, and $^{\mathrm{D}}\tilde{\sigma}_{11}^{\mathrm{b}}$ and $^{\mathrm{D}}\tilde{\sigma}_{11}^{\mathrm{nb}}$ represent the deviatoric intrinsic stresses due to bonded and nonbonded interactions, respectively. Because the deviatoric intrinsic stresses have the same magnitude in equilibrium and during α relaxation, the SOC can be evaluated from an equilibrium simulation.

3. Structural Changes during Relaxation

Atomic-Level Stress Relaxation. Figure 1 shows a typical history of the global stress difference σ^{nb} during loading and relaxation as obtained for the system with $N_{\mathrm{b}} = 10$, $\rho = 1$, and $T = 1$. The stress due to the preferential orientation of bonds ($\sigma_{\mathrm{or}}^{\mathrm{nb}}$) is also shown. This quantity is evaluated using eq 9. The constant C results from eq 10, with the intrinsic stress, $^{D}\tilde{\sigma}_{11}^{\mathrm{nb}}$, computed in equilibrium and under similar thermodynamic conditions. Only the stress produced by nonbonded interactions is considered here because that due to bonded interactions, σ^{b}, is always proportional to P_2 and hence shows no β relaxation. The global nonbonded

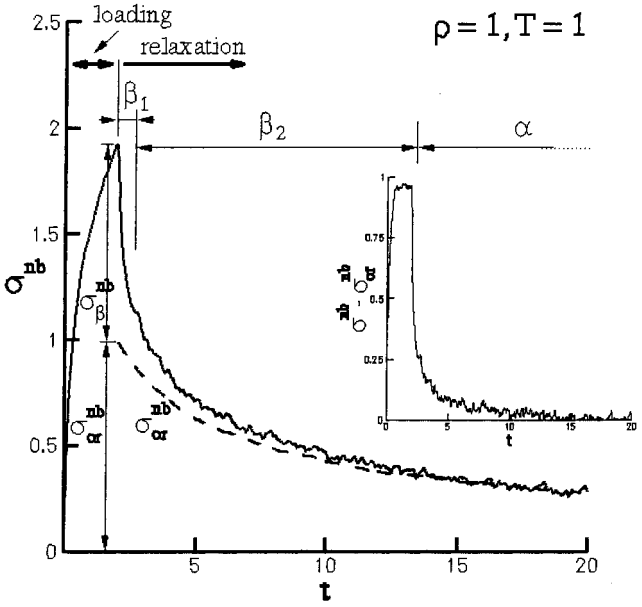

Figure 1. Time variation of the nonbonded stress difference computed in the global coordinate system during loading and relaxation. The stress induced by the preferential bond orientation, $\sigma_{\mathrm{or}}^{\mathrm{nb}}$, is shown by the dashed line. The global stress is identical to $\sigma_{\mathrm{or}}^{\mathrm{nb}}$ during the α-relaxation regime. The stress at any instant of time can be expressed as a superposition of the stress components due to three distinct stress-production mechanisms discussed in text. The inset shows the time variation of the stress produced by the mechanisms active during the β regime only.

stress becomes identical to $\sigma_{\mathrm{or}}^{\mathrm{nb}}$ at late times during the relaxation period, whereas σ^{nb} is larger at early times. This observation helps to distinguish the α relaxation (during which the preferential bond orientation is the only stress production mechanism) from the β regime. Additional deformation mechanisms are active during the β regime. This accounts for the difference between σ^{nb} and $\sigma_{\mathrm{or}}^{\mathrm{nb}}$ at early times (inset to Figure 1).

The stress relaxation during the β period shows two clearly defined regimes. The stress drops sharply within $\delta t \approx 0.2$ from the onset of relaxation at time $t = 2$. The total stress drop in this regime ($\beta 1$) is about 50% of the total stress magnitude at the beginning of the relaxation period. The time variation of stress can be described by a power law. Similar relaxation modes are usually observed experimentally at very high frequencies and are known to be associated with localized structural changes. This regime is followed by a slower exponential decay ($\beta 2$). The magnitude of the stress drop during $\beta 2$ is much smaller than that during $\beta 1$, but $\beta 2$ is slower and hence more important from a dynamic point of view.

It is also interesting to observe that the stress difference $\sigma^{\mathrm{nb}} - \sigma_{\mathrm{or}}^{\mathrm{nb}}$ (inset to Figure 1) reaches a steady state during loading ($t < 2$) and at a constant deformation strain rate. This dynamic equilibrium is reached when the deformation rate equals the rate of the β-relaxation processes. Hence, for this domain, it is possible to write $\sigma^{\mathrm{nb}} - \sigma_{\mathrm{or}}^{\mathrm{nb}} = \eta\dot{\epsilon}$, where η is a temperature- and density-dependent viscosity.

Structural Changes. The structural changes that accompany stress relaxation in simple liquids have been studied extensively.[13,17] Furthermore, it has been shown that similar phenomena take place in diatomic liquids, as well as in longer-chain polymeric systems.[8] For completeness, these findings are briefly reviewed here.

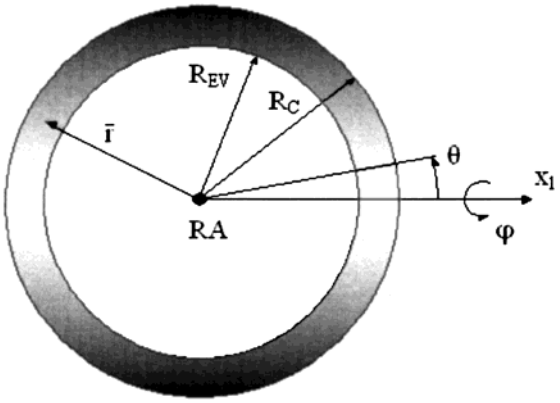

Figure 2. Schematic representations of the nonbonded-neighbor number density about a representative atom, RA, in the global coordinate system at the beginning of relaxation (t = 2 in Figure 1). Darker shades of gray represent higher densities. No neighbors are present in the close neighborhood of RA because of the strong repulsion (excluded volume). The neighborhood is shown only within a potential cutoff radius R_c from RA. The distribution has a cylindrical symmetry about the stretch direction x_1, with a higher density at $\theta = 90°$.

The equilibrium structure of the liquid is fully described on the atomic scale by the radial distribution function $g(\mathbf{r})$. In both simple and macromolecular liquids, this distribution is spherically symmetric in equilibrium. The existence of an anisotropic or nonzero deviatoric stress at the end of the loading period must be accompanied by an anisotropic, nonspherically symmetric radial distribution function $g(\mathbf{r})$. The relaxation of this stress corresponds to the return of $g(\mathbf{r})$ to isotropy. Under the elongational deformation considered here, the distribution has cylindrical symmetry. This process can be described using the concept of the "cage" of the representative atom. The "shape" of the cage is defined by the distribution $g(r,\theta)$, $0 < r < R_c$, which, in turn, can be simply described by two measures of anisotropy, $\bar{r}(\theta)$ and $\bar{N}(\theta)$. $\bar{r}(\theta)$ is the mean distance between the representative atom and the nonbonded neighbors, and $\bar{N}(\theta)$ is proportional to the number density of nonbonded atoms in the cage, both at angle θ and in the global coordinate system. These parameters are defined by[18]

$$\bar{r}(\theta) = \frac{\int_0^{R_c} r g(r,\theta) r^2 \, dr}{\int_0^{R_c} g(r,\theta) r^2 \, dr} \quad \text{and}$$

$$\bar{N}(\theta) = \frac{3}{\rho_c R_c^3} \int_0^{R_c} \rho g(r,\theta) r^2 \, dr \quad (11)$$

During loading, the equilibrium spherical shape of the cage becomes ellipsoidal with the long semi-axis in the stretch direction. This is reflected by the evolution of $\bar{r}(\theta)$. Similarly, the number density $\bar{N}(\theta)$ in the stretch direction ($\theta = 0$) becomes smaller than the equilibrium value, with the opposite trend in the $\theta = \pi/2$ direction. These changes are shown schematically in Figure 2. The distribution of nonbonded neighbors about the representative atom RA is shown by shades of gray, with darker regions corresponding to higher number densities. The distribution is shown up to R_c, the cutoff radius of the nonbonded interaction potential. The density vanishes in the central region because of the excluded-volume effect. The distribution has cylindrical symmetry about the x_1 axis.

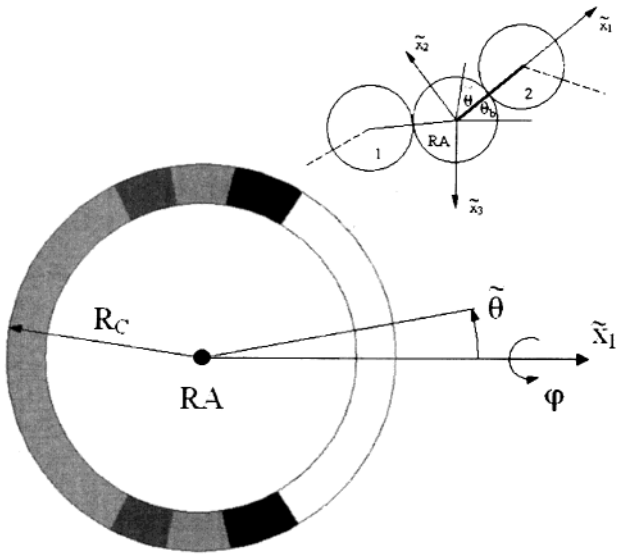

Figure 3. Schematic representations of the nonbonded-neighbor number density about a representative atom, RA, in the intrinsic coordinate system. The density vanishes in the close neighborhood of RA as a result of the excluded-volume effect and at $\tilde{\theta} = 0$, because of the steric shielding. The inset shows the intrinsic coordinate system in which the $\tilde{x}_1$ axis is tied to the bond between atoms RA and 2. The other bond, atom 1 to RA, does not have a specified position in the intrinsic frame $\tilde{x}_i$, and its shielding effect does not influence the distribution.

It has been shown that, at the beginning of the α-relaxation regime, when $\sigma^{nb} = \sigma_{or}^{nb}$ (Figure 1), the spherical symmetry of the cage is recovered. Hence, the two β-relaxation modes identified above correspond to the return to isotropy of the cage.

These quantities can also be computed in the intrinsic coordinate system. In equilibrium, the radial distribution function in this frame, $\tilde{g}(r,\theta)$, is cylindrically symmetric about the intrinsic $\tilde{x}_1$ axis tied to a covalent bond. The lack of spherical symmetry is due to the steric shielding. This effect is caused by the neighboring covalently bonded atom, which, in the intrinsic frame, preserves a fixed position with respect to RA (inset to Figure 3). Figure 3 shows a schematic representation of the intrinsic distribution. Interestingly, it was observed that this distribution changes slightly during the loading period, whereas during relaxation, it is essentially insensitive to melt deformation. This is the structural origin of the deformation-insensitive intrinsic stress tensor and the physical basis for the existence of a constant stress-optical coefficient during the α relaxation.[8]

In addition to these mechanisms, in macromolecular liquids, the bonds are preferentially oriented in the stretch direction during deformation. Because each bond carries a nonzero deviatoric stresslet (intrinsic stress tensor), the alignment produces a macroscopic deviatoric stress. This stress relaxes during the α-relaxation regime when the bond orientation distribution returns to isotropy.

This phenomenon has implications for the present discussion of β relaxation. A random orientation of bonds (intrinsic frames) would lead to a spherically symmetric neighbor distribution $g(r)$ in the global coordinate system. The magnitudes of $\bar{r}$ and $\bar{N}$ in equilibrium can be obtained by averaging the equivalent intrinsic quantities, $\tilde{r}$ and $\tilde{N}$, over all possible directions $\tilde{\theta}$ in intrinsic coordinates. When the intrinsic frames

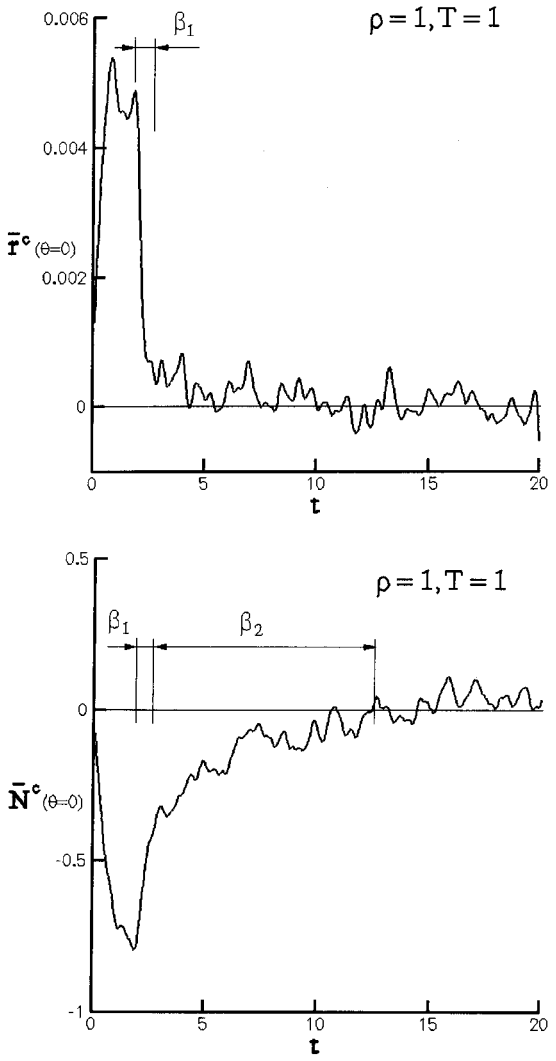

Figure 4. Time variation of (a) $\bar{r}^c$ and (b) $\bar{N}^c$ during loading and relaxation. The relaxation of $\bar{r}^c$ corresponds to the first stress relaxation regime, $\beta 1$, whereas that of $\bar{N}^c$ corresponds to $\beta 2$. The two mechanisms are essentially decoupled.

become preferentially oriented, $\bar{r}$ and $\bar{N}$ change. Hence, the two measures of eq 11 do not decay to zero by the beginning of the α regime and are dependent on the average bond orientation.

Hence, two new bond-orientation-insensitive parameters need to be developed. These "corrected" measures are obtained from those in eq 11 by subtracting the contribution due to the preferential bond orientation. Specifically, when computing the corrected measures for a given angle θ, it is necessary to subtract from the result of eq 11 at the respective θ the equivalent quantities obtained from the orientation-insensitive intrinsic distribution of Figure 3, as if all bonds would be oriented at the current bond angle θ_b. The corrected measures are

$$\bar{r}^c(\theta) = \langle \bar{r}(\theta) - \tilde{r}(\theta_b - \theta) \rangle \quad \text{and}$$
$$\bar{N}^c(\theta) = \langle \bar{N}(\theta) - \tilde{N}(\theta_b - \theta) \rangle \quad (12)$$

Here, θ_b is the angle made by the bond with the global x_1 axis, and $\tilde{r}$ and $\tilde{N}$ are averaged over all possible bond orientations ϕ at the given θ. Because θ is the only relevant angular parameter, the effect of the other Euler angle, ϕ, describing the orientation of the current intrinsic frame needs to be averaged out. The brackets represent averaging over the whole population and over all N_c replicas. Furthermore, $\tilde{r}$ and $\tilde{N}$ are computed from equilibrium and represent the deformation-insensitive intrinsic distribution, identical for equilibrium and α relaxation.

The corrected measures of eq 12 are shown in Figure 4 for the system with $N_b = 10$, $\rho = 1$, and $T = 1$ (corresponding to the data in Figure 1) and for $\theta = 0$ (in the direction of the x_1 axis). $\bar{r}^c$ reaches a steady state during loading and abruptly returns to zero after the beginning of relaxation. This is clearly associated with the $\beta 1$ regime of stress relaxation. $\bar{N}^c$ shows a slower decay and essentially vanishes by the beginning of the α relaxation at $t \approx 14$. This parameter is associated with the $\beta 2$ stress-relaxation regime.

In some situations, another parameter describing the time variation of the number density distribution $\bar{N}$ might become useful. This is the first moment of the distribution, $P_2^{nb} = {}^1/_2\langle 3\cos^2\theta_{nb} - 1\rangle$, where θ_{nb} is the angular position of a nonbonded neighbor with respect to the representative atom in global coordinates. This measure is much less noisy than $\bar{N}(\theta)$, and hence, its evaluation requires less averaging. As with the other measures of the cage shape, $\bar{r}$ and $\bar{N}$, P_2^{nb} is not independent of the average bond orientation. To filter out this effect, a correction similar to that applied to $\bar{r}$ and $\bar{N}$ is used. The corrected measure is

$$P_2^{nb\,c} = P_2^{nb} - \frac{P_2}{4}\frac{\int_0^\pi \tilde{N}(\theta)\sin\theta(1+3\cos 2\theta)\,d\theta}{\int_0^\pi \tilde{N}(\theta)\sin\theta\,d\theta} \quad (13)$$

where $\tilde{N}$ is the equilibrium number density in intrinsic coordinates and P_2 is the first moment of the bond orientation distribution, as previously defined.

Finally, the two structural relaxation mechanisms, that associated with $\bar{r}^c$ and that involving $\bar{N}^c$, are essentially decoupled. Furthermore, they are decoupled from the structural relaxation mode characteristic for the α regime (preferential bond orientation). This suggests that the total stress at any time t can be written as the superposition of the stresses produced by these three mechanisms as

$$\sigma^{nb} = \sigma^{nb}_{\beta 1} + \sigma^{nb}_{\beta 2} + \sigma^{nb}_{or} \quad (14)$$

4. $\beta 1$ Relaxation

The $\beta 1$ relaxation is a quasielastic response with a very short duration. The associated stress drop is significant: up to one-half the magnitude of the stress at the end of the loading period. The magnitude of the drop decreases with decreasing stiffness of the repulsive branch of the interatomic potential that represents nonbonded interactions. As discussed above, the parameter $\bar{r}^c$, a measure of the anisotropy of the representative atom's cage, returns to isotropy during this regime. The magnitude of the stress drop, $\sigma^{nb}_{\beta_1}$, is directly related to the magnitude of the variation of $\bar{r}^c$. Figure 5 makes explicit this relationship. In this figure, the abscissa represents the total variation of $\bar{r}^c$ measured in the stretch direction at $\theta = 0$. $\bar{r}^c$ computed in other directions θ in the global coordinate system is proportional to the value reported here and, hence, relaxes to zero within the same time interval. The data

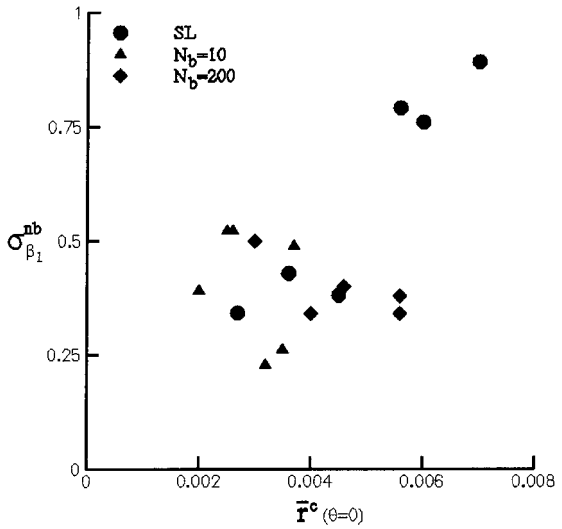

Figure 5. Magnitude of stress drop during $\beta 1$ as a function of the total variation of the anisotropy parameter $\bar{r}^c$. The data points correspond to systems of various densities, chain lengths, and temperatures.

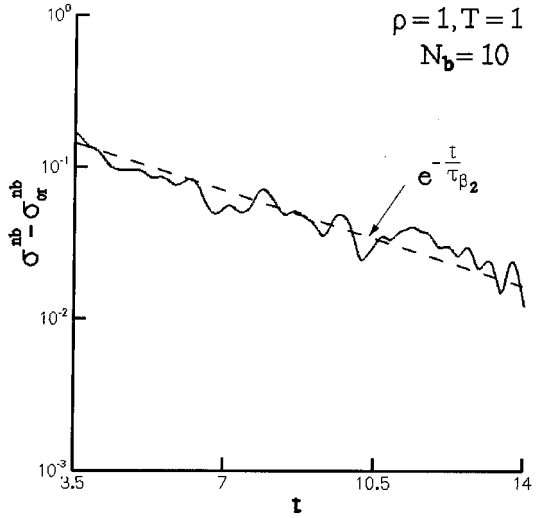

Figure 6. History of the stress difference $\sigma^{nb}_{\beta_2} = \sigma^{nb} - \sigma^{nb}_{or}$ after completion of $\beta 1$ relaxation in a semilogarithmic coordinate system. The $\beta 2$ relaxation is exponential.

points correspond to systems with various chain lengths and under various conditions of density and temperature. Notwithstanding the statistical scatter, the stress appears to be proportional to the drop in $\bar{r}^c$. Because $\bar{r}^c$ can be translated into a measure of strain (e.g., by normalization with $\bar{r}$), the observed linearity supports the conjecture regarding the quasielastic nature of the deformation during this relaxation regime. Finally, this mechanism involves only local rearrangements within the neighborhood of the representative atom, and hence, the parameters describing the $\beta 1$ mode do not scale with the chain length.

5. $\beta 2$ Relaxation

The stress-producing mechanism during $\beta 2$ is the cage anisotropy, specifically, the anisotropy in the neighbor number density $\bar{N}^c$. The stress, $\sigma^{nb}_{\beta_2} = \sigma^{nb} - \sigma^{nb}_{or}$, fully relaxes by the beginning of the α regime at $t \approx 14$ (inset to Figure 1). Figure 6 shows its time

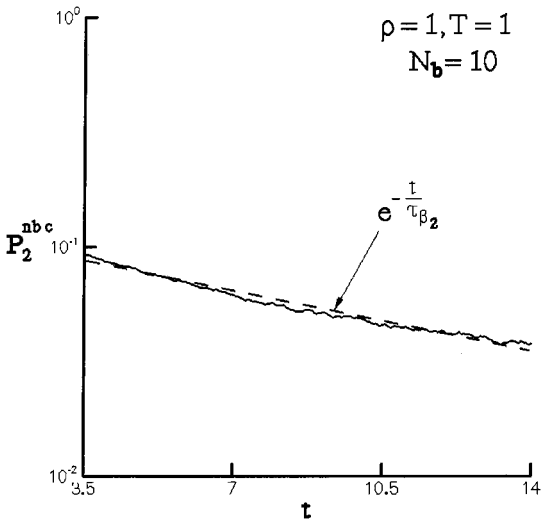

Figure 7. History of the first moment of the nonbonded-neighbor number density distribution in global coordinates. This quantity was corrected to exclude the effect of the preferential bond orientation on the distribution. The relaxation follows an exponential with a time constant similar to that describing stress relaxation (Figure 6).

variation in a semilogarithmic coordinate system for the system with $N_b = 10$. The computed stress trajectory is well approximated by an exponential with a relaxation time constant $\tau_{\beta_2} = 5.3$ (the dotted line in Figure 6).

The evolution of the neighbor number density $\bar{N}^c$ follows an exponential decay with a similar time constant. Figure 7 shows the variation of the first moment of this distribution, $P_2^{nb\,c}$ (eq 13), over the same time interval. The relaxation time constant measured from this plot ($\tau = 6$) is in good agreement with that obtained for stress relaxation. The agreement is preserved at other temperatures and densities and suggests that the stress-relaxation time constant can be predicted on the basis of the underlying mechanism. To this end, a continuum model of diffusion in the neighborhood of the representative atom is developed.

Continuum Model. The nonbonded-neighbor distribution about the representative atom and in the global coordinate system is projected onto a sphere of diameter $\bar{r}$. Here, $\bar{r}$ has the equilibrium value and is θ-independent. At the beginning of the $\beta 2$ regime, the atom number density on this sphere is nonuniform, the density being higher at the "equator" (at $\theta = 90°$) and smaller at the "poles" (along the x_1 axis) (Figure 2). The homogenization of this distribution occurs by a diffusion process that can be described by the standard diffusion equation[19]

$$\frac{\partial \bar{N}}{\partial t} = D^{\theta}\frac{1}{\bar{r}^2}\left[\frac{1}{\tan\theta}\frac{\partial \bar{N}}{\partial \theta} + \frac{\partial^2 \bar{N}}{\partial \theta^2}\right] \qquad (15)$$

Here, D^{θ} is a diffusion coefficient "on the surface of the sphere". The cylindrical symmetry of the problem was considered in writing eq 15.

The solution of eq 15, i.e., the function $\bar{N}(\theta,t)$, can be written in terms of Legendre polynomials $P_n(\cos\theta)$ as a superposition of relaxation modes ($n = 0, 2, 4, \ldots$). In particular, the various terms in the solution relax according to

$$P_n(t) = P_n(0)e^{-n(n+1)(D^{\theta}/\bar{r}^2)t} \qquad (16)$$

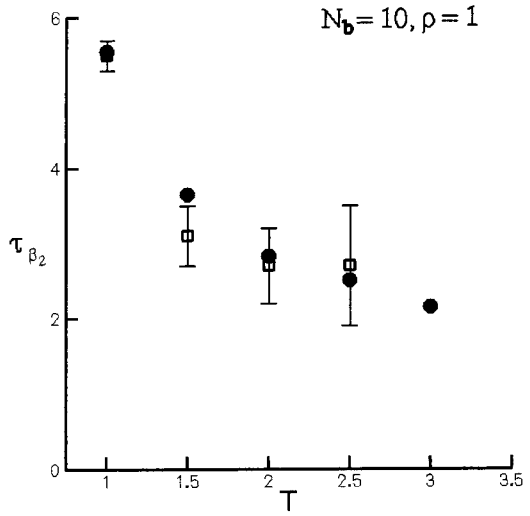

Figure 8. Comparison of relaxation time constants for the $\beta 2$ regime as evaluated from the nonequilibrium stress history (open data points and error bars) and from equilibrium simulations based on the fluctuation−dissipation theorem (eq 17). The good agreement of the two sets of data suggests that the system is in the linear-response regime during $\beta 2$.

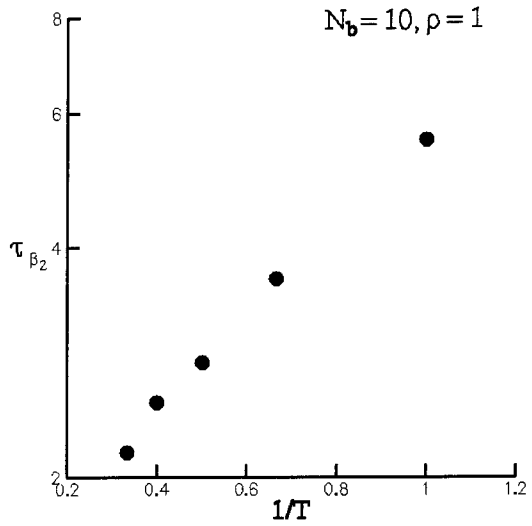

Figure 9. Arrhenius plot of the data in Figure 8. The plot shows that the $\beta 2$ relaxation is a noncooperative process involving only local structural changes. The temperature dependence of the stress relaxation time constant can be described by an Arrhenius equation.

The second term ($n = 2$) has a relaxation time constant of

$$\tau_{\beta_2} = \frac{\bar{r}^2}{6D^\theta} \tag{17}$$

Judging from the above discussion, this time constant must be similar to that characteristic for stress relaxation during the $\beta 2$ regime.

Attention is focused here on the second term in the expansion of the solution in a series of Legendre polynomials because the number density distribution $\bar{N}(\theta)$ at the beginning of $\beta 2$ is closely described by this term, namely, $P_2(\cos\theta)$. The coefficient of the next term ($n = 4$) is 2 orders of magnitude smaller than that of the second term ($n = 2$). This, in turn, suggests that the only relevant relaxation time constant for the initial distribution $\bar{N}(\theta,t_0)$ is that of eq 17.

Diffusion Coefficient. To compare the predictions of this model with the stress relaxation time constant obtained from nonequilibrium simulations, it is necessary to evaluate the diffusion constant D^θ. This parameter is computed from an equilibrium simulation using the Green−Kubo equation as[20]

$$D^\theta = \lim_{t\to\infty} \int_0^t \left(1 - \frac{s}{t}\right) \langle v^\theta(0) \cdot v^\theta(s) \rangle \, ds \tag{18}$$

Here, the angular brackets represent the velocity autocorrelation function. The autocorrelation function is computed on the basis of the tangential component of the velocity of nonbonded neighbors relative to the representative atom, v^θ (in a spherical coordinate system centered on the representative atom). The tangential component of the velocity (in the θ direction) is selected to represent the diffusion process of interest, i.e., diffusion through the relatively thin layer of interacting nonbonded neighbors about the representative atom. In the present model, this "layer" is bounded on the outside by the cutoff radius of the potential and on the inside by the excluded-volume region, and it has a thickness of about 0.18 (Figure 2). By this procedure, only those equilibrium density fluctuations whose relaxation entails relative motions of atoms that are representative for the diffusion process considered here are selected.

This diffusion coefficient was also evaluated on the basis of the angular velocity of nonbonded neighbors, ω^θ, and the results differ by less than 3%. The autocorrelation function was computed up to time $s = 0.9$, and the equilibrium simulation was run up to time 450. Hence, the upper limit of the integral in eq 18 was actually taken to be 0.9. It was verified that selecting an upper limit of 0.8 did not significantly affect the computed diffusion coefficient.

Comparison with Nonequilibrium Simulation Results. Equations 17 and 18 were used to estimate the stress relaxation time constant τ_{β_2} at various temperatures for the dense system with $N_b = 10$ and $\rho = 1$. The results are shown in Figure 8, along with the relaxation time constant measured from the nonequilibrium stress history. The error bars are a measure of the effect of statistical noise on the time constant evaluated in nonequilibrium simulations. The noise and the error bars increase with temperature, as expected. It was found necessary to average over 200 replicas of the system and to subsequently use a low-pass filter on the averaged stress before attempting to extract the relaxation time constants reported here.

The two sets of data in Figure 8 are in good agreement, which suggests that the $\beta 2$ relaxation is indeed controlled by the diffusion-like process described above. More importantly, the fact that the nonequilibrium time constant can be predicted from equilibrium using the fluctuation−dissipation theorem suggests that the system is in the linear-response regime during $\beta 2$. It is known that the diffusion coefficients obtained using the Green−Kubo equation, i.e., in the limit of infinitesimal perturbations, are usually smaller than those estimated from nonequilibrium simulations.[21] This situation would lead to the time constants computed from equilibrium (the closed points in Figure 8) being slightly larger than those evaluated in nonequilibrium. This effect is not clearly observed here because of the relatively large error bars on the nonequilibrium quantities.

Insight into the nature of this relaxation process can be gained by plotting the time constants in an Arrhenius

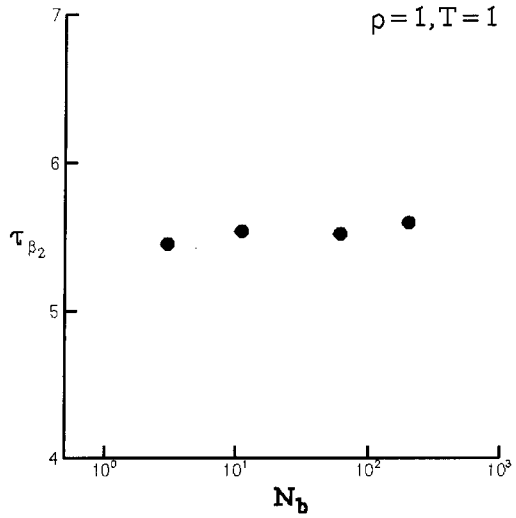

Figure 10. Dependence of the stress relaxation time constant for $\beta 2$ on chain length. The abscissa represents the number of bonds per chain. The time constant is essentially chain-length-independent, which supports the conclusion that processes taking place during the $\beta 2$ relaxation are noncooperative.

plot (Figure 9). The data points obtained using eqs 17 and 18 align, which suggests that this is a simple thermally activated process involving only local structural changes.[22,23]

To test the noncooperative nature of the process, the scaling of the relaxation time constant with chain length was studied. Figure 10 shows the time constants evaluated from equilibrium in the dense state at $\rho = 1$ and $T = 1$ for systems with various chain lengths ($N_b = 1$, 10, 60, and 200). τ_{β_2} appears to be essentially chain-length-independent. This conclusion can also be obtained by carefully analyzing the nonequilibrium stress histories for the various systems. This observation supports that obtained from the Arrhenius plot of Figure 9.

6. Conclusions

The β relaxation in the model polymeric system studied here encompasses two modes, $\beta 1$ and $\beta 2$. The $\beta 1$ mode is a quasielastic rebound and cannot be described by an exponential function. It involves only local structural changes of the fluid. A significant fraction of the total stress relaxes during this regime. The $\beta 2$ mode is exponential and is associated with a diffusion process by which the neighborhood of a representative atom (the cage) recovers its spherical symmetry characteristic for the equilibrium state. The relaxation time constant for this mode can be predicted from equilibrium using a mechanism-based model. This suggests that the system is in the nonequilibrium linear-response regime during $\beta 2$. The temperature dependence of the $\beta 2$ relaxation time constant is described by an Arrhenius law, for which the time constant is also chain-length-independent.

Acknowledgment. This work was supported by the NSF through Grant CMS-9908025.

References and Notes

(1) Rouse, P. E. *J. Chem. Phys.* **1953**, *21*, 1272−1285.
(2) Doi, M.; Edwards, S. F. *The Theory of Polymer Dynamics*; Clarendon Press: Oxford, U.K., 1986.
(3) Bird, R. B.; Curtis, C. F.; Armstrong, R. C.; Hassager, O. *Dynamics of Polymeric Liquids: Kinetic Theory*; Wiley-Interscience: New York, 1987.
(4) Gao, J.; Weiner, J. H. *Macromolecules* **1996**, *29*, 6048−6055.
(5) Gao, J.; Weiner, J. H. *Macromolecules* **1992**, *25*, 3462−3467.
(6) Loriot, G.; Weiner, J. H. *J. Polym. Sci: Polym. Phys.* **1998**, *36*, 143−154.
(7) Picu, R. C.; Loriot, G.; Weiner, J. H. *J. Chem. Phys.* **1999**, *110*, 4678−4686.
(8) Picu, R. C. *Macromolecules* **1999**, *32*, 7319−7324.
(9) Gao, J.; Weiner, J. H. *J. Chem. Phys.* **1989**, *90*, 6749−6760.
(10) Gao, J.; Weiner, J. H. *Science* **1994**, *266*, 748−751.
(11) Kroger, M.; Luap, C.; Muller, R. *Macromolecules* **1997**, *30*, 526−539.
(12) Picu, R. C. *Macromolecules* **2001**, *34*, 5023−5029.
(13) Picu, R. C.; Weiner, J. H. *J. Chem. Phys.* **1998**, *108*, 4984−4991.
(14) Berendsen, H.; Postma, J.; van Gunsteren, W. *J. Chem. Phys.* **1984**, *81*, 3684−3693.
(15) Swenson, R. W. *Am. J. Phys.* **1987**, *55*, 746−751.
(16) Gao, J.; Weiner, J. H. *Macromolecules* **1994**, *27*, 1201−1209.
(17) Heyes, D. M.; Montrose, C. J.; Litovitz, T. A. *J. Chem. Soc., Faraday Trans.* **1983**, *79*, 611−635. Heyes, D. M.; Kim, J. J.; Montrose C. J.; Litovitz, T. A. *J. Chem. Phys.* **1980**, *73*, 3987−3995.
(18) Picu, R. C.; Weiner, J. H. *J. Chem. Phys.* **1997**, *107*, 7214−7222.
(19) Pipes, L. A.; Harvill, L. R. *Applied Mathematics for Engineers and Physicists*; McGraw-Hill: New York, 1970.
(20) Reif, F. *Fundamentals of Statistical and Thermal Physics*; McGraw-Hill: New York, 1965.
(21) Hoover, W. G. *Molecular Dynamics*; Springer-Verlag: New York, 1986.
(22) Starkweather, H. W. *Macromolecules* **1988**, *21*, 1798−1802.
(23) Mano, J. F.; Lanceros-Mendez, S. *J. Appl. Phys.* **2001**, *89*, 1844−1849.

MA0115949